Dynamical leakage of Majorana mode into side-attached quantum dot

J. Barański [1,*], M. Barańska [1], T. Zienkiewicz,[1] R. Taranko,[2] and T. Domański [2,†]

[1]*Department of General Education, Military University of Aviation, ulica Dywizjonu 303, 08-521 Dęblin, Poland*
[2]*Institute of Physics, M. Curie-Skłodowska University, 20-031 Lublin, Poland*

We study a hybrid structure, comprising a single-level quantum dot attached to a topological superconducting nanowire, analyzing dynamical transfer of the Majorana quasiparticle onto the normal region. Motivated by the recent experimental realization of such a heterostructure and its investigation under stationary conditions [Schneider *et al.*, Nat. Commun. **11**, 4707 (2020)] where the quantum dot energy level can be tuned by gate potential, we examine how much time is needed for the Majorana mode to leak into the normal region. We estimate that for typical hybrid structures this dynamical process would take about 20 ns. We propose a feasible empirical protocol for its detection by means of the time-resolved Andreev tunneling spectroscopy.

I. MOTIVATION

Topological superconductors, hosting the Majorana boundary modes, are currently of interest both for basic science [1–3] and for potential applications [4,5]. Topological protection and a non-Abelian character make them promising candidates for the realization of stable qubits [6] and quantum computations [7]. Signatures of their fractional statistics can be tested, for instance, by a sequence of charge-transfer operations using the quantum dots attached to a topological superconductor [8–10]. Such dynamical transfer of the charge between the quantum dot and topological superconductors might enable non-Abelian operations on the Majorana bound states [11,12].

Development of time-resolved spectroscopies with their resolution down to the subpicosecond regime allows us to probe the physical structures in response to an abrupt change in the model parameter(s) or other nonequilibrium conditions [13]. Such dynamics was recently investigated in topological phases by a number of groups considering fermionic [14–16] and bosonic [17] systems. In particular, dynamical teleportation due to the nonlocality of the zero-energy boundary modes has been explored [18], and it has been shown that dynamical techniques based on the noise measurements could unambiguously identify the true Majorana quasiparticles [19–22]. Time-dependent measurements have also been proposed to detect topological invariants of the higher-order topological superconductor, harboring the corner states [23].

Hybrid structures consisting of the topological superconducting nanowires side attached to the quantum dots allow for tunable control of the zero-energy bound states [24–26]. Their variations with respect to the gate potentials or magnetic field could discriminate the true Majorana quasiparticles from the trivial Andreev bound states, appearing accidentally at zero energy [27]. More complex magnetic-superconducting heterostructures enable the coexistence of the localized and chiral modes [28].

Here we analyze a dynamical transfer of the Majorana mode from the superconducting nanowire to the quantum dot (Fig. 1) driven by (i) their sudden coupling and (ii) an abrupt change in the quantum dot (QD) energy level imposed by an external gate potential. We examine the characteristic timescales associated with such dynamical Majorana leakage into the quantum dot region and show that a time-resolved process provides valuable insight into effective quasiparticles of the topological hybrid structures.

This paper is organized as follows. In Sec. II we introduce the microscopic model and outline the procedure for studying the time-dependent evolution. Next, in Sec. III, we consider dynamical properties of the quantum dot isolated from the normal lead, $\Gamma_N = 0$, or superconducting lead, $\Gamma_S = 0$. Section IV presents the time-dependent signatures of the Majorana quasiparticle leaking onto the quantum dot for the setup sketched in Fig. 1. In Sec. V we provide realistic estimations of the characteristic time and energy scales which could be practically verified experimentally. Finally, Sec. VI summarizes the main results.

II. FORMULATION OF THE PROBLEM

We study dynamical properties of the heterostructure comprising the quantum dot deposited on an *s*-wave superconductor and weakly coupled to another metallic lead that can be thought of as a scanning tunneling microscope (STM) tip. The quantum dot is additionally coupled to the topological superconducting nanowire, hosting the Majorana end modes (Fig. 1). Our considerations aim to determine the characteristic time needed for development of the Majorana features transmitted into the QD region. In particular, we shall investigate (i) the quantum evolution driven by the abrupt formation of the hybrid structure, inspecting the zero-energy features appearing for various positions of the quantum dot energy level, and (ii) how long it takes to qualitatively

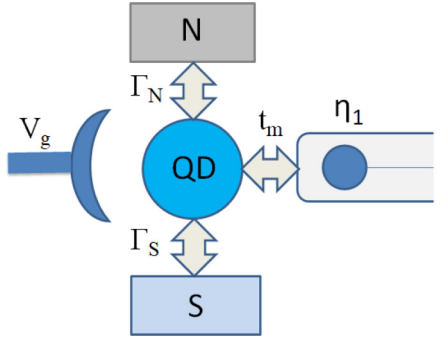*j.baranski@law.mil.pl
†doman@kft.umcs.lublin.pl

FIG. 1. Schematic representation of the considered system comprising a quantum dot (QD) deposited between metallic (N) and superconducting (S) electrodes and side coupled to one end of a monoatomic chain hosting Majorana edge state represented by η_1. The additional electrode stands for gate voltage V_g tuning of the quantum dot's energy level.

transform the existing Majorana signatures after a sudden change in the QD level.

It was predicted [29] that in a QD attached to a topological superconductor the zero-energy quasiparticle would be transmitted to the normal region. The first empirical evidence for such Majorana leakage was reported by Deng *et al.* [24] and was recently reported for the STM method by Schneider *et al.* [26]. Quantum-dot–topological-superconductor hybrid structures have been studied by a number of groups (see Ref. [30] for a survey). In N-QD-S configurations (where N indicates a normal metal and S is a superconductor; Fig. 1) such a leakage process qualitatively depends on the QD level [31,32]. Namely, when the energy level is away from zero, the signatures of the Majorana mode are manifested by the peak appearing in the density of states, thereby enhancing the zero-bias conductance. Contrary to such a picture, when the QD level happens to be near zero energy, the quantum interference induces the fractional Fano-type depletion in the QD spectrum [33]. Dynamical changeover from one regime to another has not been analyzed yet, and that is the main purpose of our present study.

A. Microscopic scenario

Let us start by formulating the microscopic model and presenting the computational method used for the determination of time-dependent quantities. We describe our hybrid structure (Fig. 1) by the following Hamiltonian:

$$\hat{H} = \hat{H}_{\text{QD}} + \sum_\beta (\hat{H}_\beta + \hat{T}_{\text{QD}-\beta}) + \hat{H}_{\text{MQD}}, \qquad (1)$$

where $\hat{H}_{\text{QD}}$ refers to the QD, $\hat{H}_\beta$ denote the metallic ($\beta = N$) and superconducting ($\beta = S$) leads, and $\hat{H}_{\text{MQD}}$ stands for the zero-energy Majorana quasiparticles and coupling of one of them to the QD. The normal lead can be treated as a Fermi sea, $\hat{H}_N = \sum_{k,\sigma} \xi_{Nk} \hat{c}^\dagger_{Nk\sigma} \hat{c}_{Nk\sigma}$, where $\hat{c}^\dagger_{Nk\sigma}$ ($\hat{c}_{Nk\sigma}$) is the creation (annihilation) operator of the σ spin electron whose energy $\xi_{Nk} = \varepsilon_{Nk} - \mu_N$ is measured from the chemical potential μ_N. The superconducting electrode is taken in BCS-type form, $\hat{H}_S = \sum_{k,\sigma} \xi_{Sk} \hat{c}^\dagger_{Sk\sigma} \hat{c}_{Sk\sigma} - \sum_k (\Delta_S \hat{c}^\dagger_{Sk\uparrow} \hat{c}^\dagger_{Sk\downarrow} + \text{H.c.})$, where Δ_S is the isotropic pairing gap. Itinerant electrons are hy-

bridized with the quantum dot through the term $\hat{T}_{\text{QD}-\beta} = \sum_{k,\sigma} (V_{\beta k} \hat{d}^\dagger_\sigma \hat{c}_{\beta k\sigma} + \text{H.c.})$. We introduce the coupling functions $\Gamma_\beta = 2\pi \sum_k |V_{\beta k}|^2 \delta(\omega - \xi_{\beta k})$, assuming them to be constant in the low-energy regime.

In regard to the quantum dot we represent it by the single-level impurity term $\hat{H}_{\text{QD}} = \sum_\sigma \epsilon_d \hat{d}^\dagger_\sigma \hat{d}_\sigma$, where $\hat{d}^\dagger_\sigma$ ($\hat{d}_\sigma$) is the creation (annihilation) operator of spin $\sigma = \uparrow, \downarrow$ electrons. We focus on the low-energy regime $|\omega| \ll \Delta_S$, where the fermion degrees of freedom outside the pairing gap can be integrated out. Their influence simplifies to the induced pairing $\hat{H}_S + \hat{T}_{\text{QD}-S} \approx \Delta_d (\hat{d}_\downarrow \hat{d}_\uparrow + \text{H.c.})$ with the on-dot potential $\Delta_d = \Gamma_S/2$ [34–36].

The "proximitized" QD is thus effectively modeled by

$$\hat{H}_{\text{QD}} + \hat{H}_S + \hat{T}_{\text{QD}-S} = \sum_\sigma \epsilon_d \hat{d}^\dagger_\sigma \hat{d}_\sigma + \Delta_d (\hat{d}_\downarrow \hat{d}_\uparrow + \text{H.c.}). \quad (2)$$

Restricting our considerations to the low-energy regime (within meV around the chemical potential), we describe the topological superconductor by

$$\hat{H}_{\text{MQD}} = i\epsilon_m \hat{\eta}_1 \hat{\eta}_2 + \lambda(d_\uparrow \hat{\eta}_1 + \hat{\eta}_1 \hat{d}^\dagger_\uparrow), \qquad (3)$$

where the self-Hermitian operators $\hat{\eta}_1$ and $\hat{\eta}_2$ represent the Majorana end modes and ϵ_m stands for their overlap. The last part appearing in Eq. (3) accounts for hybridization of the left-hand side Majorana quasiparticle with the quantum dot, where λ is the coupling strength. For convenience we recast the Majorana operators by the standard fermion operators defined via $\hat{\eta}_1 = \frac{1}{\sqrt{2}}(\hat{f} + \hat{f}^\dagger)$, $\eta_2 = \frac{-i}{\sqrt{2}}(f - f^\dagger)$. This transformation implies that (3) can be rewritten as

$$\hat{H}_{\text{MQD}} = \epsilon_m \hat{f}^\dagger \hat{f} + t_m (\hat{d}^\dagger_\uparrow - \hat{d}_\uparrow)(\hat{f} + \hat{f}^\dagger) \qquad (4)$$

with the shorthand notation $t_m = \lambda/\sqrt{2}$.

B. Outline of the computational method

Fingerprints of the Majorana mode can be practically observed in the quantum dot region by examining the charge current $I_\sigma(V, t)$ induced via a N-QD-S junction by the bias voltage V. Its differential conductance $G_\sigma(V, t) = \frac{d}{dV} I_\sigma(V, t)$ can be obtained numerically using the following expression for the current:

$$I_\sigma(V, t) = -e \left\langle \frac{d\hat{N}_{N\sigma}}{dt} \right\rangle = -\frac{ie}{\hbar} \langle [\hat{H}, \hat{N}_{N\sigma}] \rangle. \qquad (5)$$

Since all parts of the Hamiltonian (1), except $\hat{T}_{\text{QD}-N}$, commute with the number operator $\hat{N}_{N\sigma}$, the tunneling current (5) reads

$$I_\sigma(V, t) = \frac{-ie}{\hbar} \sum_k [V_{Nk} \langle \hat{d}^\dagger_\sigma(t) \hat{c}_{Nk\sigma}(t) \rangle - \text{H.c.}]$$

$$= \frac{2e}{\hbar} \text{Im} \left[\sum_k V_{Nk} \langle \hat{d}^\dagger_\sigma(t) \hat{c}_{Nk\sigma}(t) \rangle \right]. \qquad (6)$$

To simplify the notation, from now on we set $\hbar = e = 1$. Additionally, we choose the chemical potential of the superconductor as a convenient reference level ($\mu_S = 0$); thus, a biased setup is characterized by $\mu_N = eV$. Since the itinerant electrons refer here solely to the metallic lead, for brevity we skip the subindex N appearing in $\hat{c}^{(\dagger)}_{Nk\sigma}$, V_{Nk}, and ξ_{Nk}.

Using the standard expression for $\hat{c}_{k\sigma}(t)$ [37],

$$\hat{c}_{k\sigma}(t) = \hat{c}_{k\sigma}(0)e^{-i\xi_k t} - iV_k \int_0^t d\tau\, e^{-i\xi_k(t-\tau)}\hat{d}_\sigma(\tau), \quad (7)$$

and imposing the wide band limit approximation, we get

$$I_\sigma(t) = 2\text{Im}\left[\sum_k V_k \langle \hat{d}_\sigma^\dagger(t)\hat{c}_{k\sigma}(0)\rangle - i\frac{\Gamma_N}{2}\langle \hat{n}_\sigma(t)\rangle\right]. \quad (8)$$

Here $\langle \cdots \rangle$ denotes the statistically averaged value. In order to determine the current (6) one needs the correlation function $\langle \hat{d}_\sigma^\dagger(t)\hat{c}_{k\sigma}(0)\rangle$ and the time-dependent QD occupancy $\langle \hat{d}_\sigma^\dagger(t)\hat{d}_\sigma(t)\rangle \equiv n_\sigma(t)$.

To find these quantities we employ the equation of motion approach [37] and make use of the fourth-order Runge-Kutta method to solve numerically the appropriate set of differential equations. Traditionally, such a procedure applied to any correlation function generates a sequence of additional functions for which the next equations of motion must be constructed until they are finally closed (or terminated). For the uncorrelated QD embedded in our heterostructure this approach mixes the operators $\hat{d}_\sigma^{(\dagger)}$ and $\hat{f}^{(\dagger)}$ with the operators of the normal lead electrons. They have the form $\sum_k V_k \langle \hat{O}(t)\hat{c}_{k\sigma}(0)\rangle$, where $\hat{O}$ stands for one of the following six operators: $\hat{d}_\downarrow$, $\hat{d}_\downarrow^\dagger$, $\hat{d}_\uparrow$, $\hat{d}_\uparrow^\dagger$, $\hat{f}$, and $\hat{f}^\dagger$. We thus have to determine 12 momentum-dependent correlation functions $f_{ki}(t) = \langle \hat{O}(t)\hat{c}_{k\sigma}(0)\rangle$ and 9 momentum-independent expectation values $f_i(t) = \langle \hat{O}(t)\hat{\bar{O}}(t)\rangle$, which are listed explicitly in the Appendix (see Table II).

In our treatment the parameters, such as the coupling t_m and the energy level ϵ_σ, can either be static or may depend on time in an arbitrary way. For a numerical solution of the coupled differential equations (A1) and (A2) we assumed the initial empty quantum dot $n_\sigma(0) = 0$ and imposed $\langle \hat{f}^\dagger(0)\hat{f}(0)\rangle = 1$. We assume that at $t = 0$ the constituents of our setup were disconnected from each other; therefore, initial values of the functions $f_{4-9}(0)$ and $f_{ki}(0)$ were zero.

III. DYNAMICS OF AN ISOLATED QD

To understand the typical timescales (discussed in Sec. IV) it would be instructive to consider first the dynamics of a quantum dot isolated from external lead(s). In the case $\Gamma_N = 0$ one can analytically determine the time-dependent operators $\hat{d}_\sigma^\dagger(t)$, $\hat{d}_\sigma(t)$, $\hat{f}^\dagger(t)$, and $\hat{f}(t)$, solving the Heisenberg equations with the use of the Laplace transforms [37]. The general analytical expressions are rather lengthy; therefore, we restrict ourselves to the time-dependent observables for $\varepsilon_d = 0$. The QD operators then take the following form:

$$\hat{d}_\uparrow(t) = \hat{d}_\uparrow(0)\frac{1}{2}\mathcal{L}_3(t) + \hat{d}_\downarrow(0)\frac{i\omega_1}{2}\mathcal{L}_2(t)$$

$$+ \hat{d}_\uparrow^\dagger(0)\frac{1}{2}\mathcal{L}_4(t) - \hat{d}_\downarrow^\dagger(0)\frac{i\omega_1}{2}\mathcal{L}_1(t)$$

$$+ [\hat{f}(0) + \hat{f}^\dagger(0)]\frac{it_m}{2}[\mathcal{L}_2(t) - \mathcal{L}_1(t)], \quad (9)$$

where

$$\mathcal{L}_{1/2}(t) = \frac{\sin(\omega_1 t)}{\omega_1} \pm \frac{\sin(\omega_2 t)}{\omega_2}, \quad (10)$$

$$\mathcal{L}_{3/4}(t) = \cos(\omega_1 t) \pm \cos(\omega_2 t), \quad (11)$$

and $\omega_1 = \Delta_d$, $\omega_2 = \sqrt{\Delta_d^2 + 4t_m^2}$. Using $\hat{d}_\uparrow^\dagger(t) = [\hat{d}_\uparrow(t)]^\dagger$, we can express the QD occupancy by

$$n_\uparrow(t) = n_\uparrow(0)\frac{1}{4}[\cos(\omega_1 t) + \cos(\omega_2 t)]^2$$

$$+ n_\downarrow(0)\frac{1}{4}\left[\sin(\omega_1 t) - \frac{\omega_1}{\omega_2}\sin(\omega_2 t)\right]^2$$

$$+ [1 - n_\downarrow(0)]\frac{1}{4}\left[\sin(\omega_1 t) + \frac{\omega_1}{\omega_2}\sin(\omega_2 t)\right]^2$$

$$+ [1 - n_\uparrow(0)]\frac{1}{4}[\cos(\omega_1 t) - \cos(\omega_2 t)]^2$$

$$+ \frac{t_m^2}{\omega_2^2}\sin^2(\omega_2 t). \quad (12)$$

Equation (12) shows that QD occupancy oscillates in time with the characteristic frequencies dependent on t_m and $\Delta_d = \Gamma_S/2$. Similar harmonic oscillations occur in the correlation functions as well. As a useful example we present the mixed function $\langle d_\uparrow^\dagger(t)f(t)\rangle$ obtained for $n_\sigma(0) = 0$, assuming $n_f(t = 0) \equiv \langle \hat{f}^\dagger(0)\hat{f}(0)\rangle = 1$,

$$\langle \hat{d}_\uparrow^\dagger(t)f(t)\rangle = i\frac{t_m}{\omega_2}\sin(\omega_2 t)\cos^2\left(\frac{\omega_1}{2}t\right)$$

$$- i\frac{\omega_1 t_m}{\omega_2^2}\sin(\omega_1 t)\sin^2\left(\frac{\omega_2}{2}t\right). \quad (13)$$

A. The case with $\Gamma_N = 0$, $\Gamma_S = 0$

Let us focus on the simplest possible case, when the QD is completely isolated from both external reservoirs ($\Gamma_N = 0 = \Gamma_S$) and it is coupled (at $t = 0$) solely to the Majorana mode. For the initial condition $n_\sigma(0) = 0$ the analytic expression (12) simplifies to $\sin^2(t_m t)$, whereas the mixed function (13) becomes $\frac{i}{2}\sin(2t_m t)$. Under such circumstances both these expectation values evolve in time through harmonic oscillations with the characteristic period $T = \frac{\pi}{t_m}$. The dot-chain coupling t_m is thus a natural unit for the frequency of quantum oscillations. It is worth noticing that for exemplary coupling $t_m = 1\,\mu\text{eV}$ the period of such oscillations would be about 2 ns.

This timescale, however, does not refer to stable development of the Majorana mode in the quantum dot spectrum because the charge oscillates back and forth between the dot and chain. To achieve such stationary limit Majorana leakage (reported experimentally [24,26]) one needs some relaxation processes. They can be provided by coupling the quantum dot to a continuum spectrum of the metallic lead or by activating the quasiparticle states of a superconductor from outside the pairing gap (the latter would be hardly probable at temperatures safely lower than T_c). Figure 2 presents the damped quantum oscillations computed numerically for the QD occupancy and the correlation function for a few finite values of Γ_N. We note that if the coupling Γ_N is comparable to t_m, the expectation values reach their equilibrium within the timescale comparable to the period of a single oscillation. We clearly notice that by connecting the dot to a continuum the
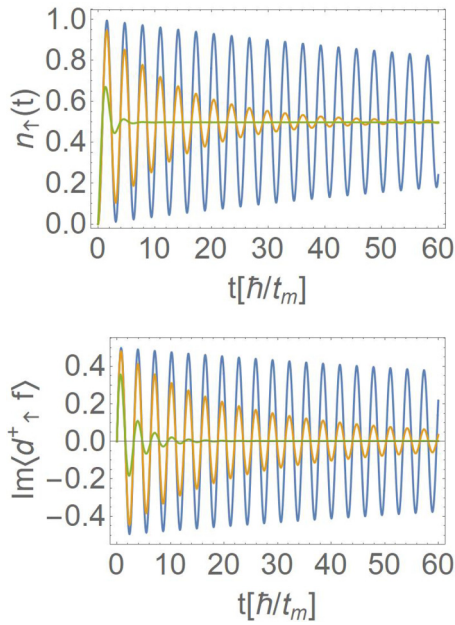
FIG. 2. The time-dependent QD occupancy $n_\uparrow(t)$ (top) and imaginary part of the mixed function $\langle \hat{d}_\uparrow^\dagger(t)\hat{f}(t)\rangle$ (bottom) obtained in the absence of the superconducting lead ($\Gamma_S = 0$) for $\epsilon_d = 0$, assuming $\Gamma_N/t_m = 0.01$ (blue line), 0.1 (orange line), and 1 (green line). Bias voltage is assumed to be zero.

hybrid structure gradually evolves towards its stationary limit via a sequence of the damped quantum oscillations with an exponential factor $e^{-\Gamma_N t}$, preserving their period.

B. The case with $\Gamma_N = 0$, $\Gamma_S \neq 0$

Taking into account the coupling of the QD to the superconducting lead ($\Gamma_S \neq 0$) the time-dependent QD occupancy is a superposition of two quantum oscillations with frequencies ω_1 and ω_2 [see Eq. (12)]. In particular, for the initial conditions $n_\sigma(0) = 0$ and $n_f(0) = 1$ one obtains

$$n_\uparrow(t) = \frac{1}{2}\left[1 - \cos(\omega_1 t)\cos(\omega_2 t) + \frac{\omega_1}{\omega_2}\sin(\omega_1 t)\sin(\omega_2 t)\right].$$
(14)

This time dependence originates from electron oscillations (i) between the quantum dot and topological chain and (ii) between the quantum dot and superconducting substrate. Physically, they manifest dynamical interplay between the zero-energy Majorana mode (of the topological nanowire) and a pair of finite-energy Andreev states (of QD proximitized to a conventional superconductor). Interference of such oscillations with different frequencies gives rise to the appearance of the beating pattern, whose period is approximately equal to π/Δ_d. Such an effect is illustrated by the blue line in Fig. 3. In the absence of the metallic lead ($\Gamma_N = 0$) this oscillatory behavior is not damped; that is, the charge occupancy of the QD does not saturate to any equilibrium value. Equilibration could eventually be achieved by coupling the quantum dot to a continuum spectrum of the metallic lead. Illustration of such an effect is presented by the orange line in Fig. 3 obtained numerically for $\Gamma_N = 0.1 t_m$. The coupling Γ_N can
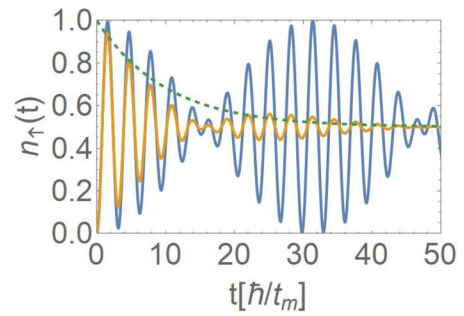

FIG. 3. The time-dependent occupancy $n_\uparrow(t)$ obtained analytically for $\Gamma_N = 0$ (blue line) and numerically for $\Gamma_N = 0.1 t_m$ (orange line), assuming $\epsilon_d = 0$, $\Delta_d = 0.1 t_m$. The green dashed line is the envelope function $\frac{1}{2}(1 + e^{-\Gamma_N t})$ due to the relaxation caused by the continuum states of the metallic lead.

hence be regarded as the relevant energy unit, characterizing the efficiency of the relaxation processes.

Although the influence of the Majorana mode on the quantum dot is not prevented in the absence of the metallic lead ($\Gamma_N = 0$), the stationary buildup of such a quasiparticle can be realized only when the relaxation processes occur. We have shown in this section that such dynamics would be characterized by two typical timescales: (i) quantum oscillations (whose period depends on t_m) and (ii) the Majorana quasiparticle development (governed by Γ_N). In particular, when Γ_N is comparable to t_m, the relaxation time might be comparable to the period of quantum oscillations. Below we show that both these timescales would be observable in the tunneling conductance.

IV. TIME-RESOLVED MAJORANA FEATURES

The most profound consequence of bringing the quantum dot in contact with a topological superconductor is the emergence of the zero-energy quasiparticle in the spectrum of the QD. This feature (measurable by charge transport through the N-QD-S circuit) is a signature of the Majorana mode. The dynamical leakage process provides information about the time required to perform logical operations with the use of the Majorana quasiparticles.

A. Dynamical Majorana leakage

Let us estimate the time required to transfer the zero-energy mode onto the QD region after abruptly coupling the quantum dot to the topological chain. Until $t = 0$ all parts of our setup (Fig. 1) are assumed to be completely disconnected, and the quantum dot is unoccupied. Thus, our initial conditions are $\langle \hat{d}_\sigma^\dagger(0)\hat{d}_\sigma(0)\rangle = 0$, $\langle \hat{d}_\downarrow(0)\hat{d}_\uparrow(0)\rangle = 0$, $\langle \hat{c}_{k\sigma}^\dagger(0)\hat{c}_{k\sigma}(0)\rangle = f_{FD}(\varepsilon_k - eV)$, and the mixed terms $\langle \hat{O}(0)\hat{c}_{k\sigma}(0)\rangle = 0$. At $t = 0^+$ the QD is abruptly connected to external reservoirs by the couplings Γ_β. To ensure the subgap quasiparticle states are well separated, we impose the asymmetric couplings ($\Gamma_S = 3\Gamma_N$). The superconducting proximity leads to a gradual buildup of the in-gap Andreev bound states. We noticed that these states reach their equilibrium positions and amplitudes after time $t \simeq \hbar/\Gamma_N$ [37].

Later, after the Andreev states are safely stabilized, we abruptly connect the quantum dot to the topological super-
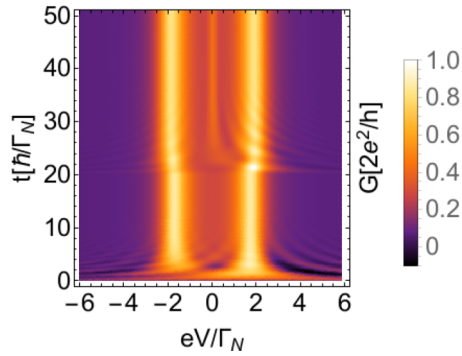
FIG. 4. The time-dependent differential conductance as a function of bias V (horizontal axis) and time t (vertical axis) obtained for $\epsilon_d = \Gamma_N$. At $t = 0$ the quantum dot is abruptly connected to the external leads (imposing $\Gamma_S = 3\Gamma_N$) when the Andreev bound states (ABSs) begin to emerge. Once the position and amplitude of ABSs are established at $t = 20\hbar/\Gamma_N$, the quantum dot is additionally connected to the topological superconductor, assuming $t_m = 0.5\Gamma_N$. From this moment onward the zero-energy peak gradually emerges, signalizing the Majorana leakage into the quantum dot region. For the chosen set of model parameters this zero-energy feature stabilizes its shape after approximately 15–20 units of time, i.e., at $t \simeq 40\hbar/\Gamma_N$.

conductor. For computations we assume $t_m = 0.5\Gamma_N$, but a more detailed discussion of the influence of t_m on the time required for the Majorana zero mode (MZM) to leak onto the QD region is given in Sec. V B. Starting from $t = 20\hbar/\Gamma_N$, the Majorana mode gradually leaks to the QD region, as manifested by the enhancement of the zero-bias conductance (Fig. 4). We can notice that its amplitude is established within the time interval $\Delta t \sim 15 - 20\hbar/\Gamma_N$. This result brings us the needed information on the characteristic time of the Majorana leakage. We need to keep in mind, however, that the coupling of the QD to the metallic reservoir Γ_N in different experimental realizations can take various values. To estimate the order of magnitude of the leakage time (in nanoseconds), in Sec. V A we compare the qualitative results with typical energy scales used in experiments on in-gap states and hybrids comprising quantum dots and topological superconducting chains.

B. Quench-driven dynamics

The transient evolution discussed in Sec. IV A allowed us to estimate the time required for the MZM leakage. Abrupt coupling of the QD to the topological superconductor would, however, hardly be feasible in practice. A more realistic scenario could rely on employing the gate voltage potential to vary the QD's energy level in a controlled manner. Depending on the specific value of ϵ_d, the Majorana mode should be evidenced either by the interferometric depletion (when $\epsilon_d \simeq 0$) or constructive enhancement (for $|\epsilon_d| \gg t_m$) of the zero-bias tunneling conductance [31,32]. To provide an experimentally verifiable result we propose to test how long it takes to transform the ditch into the peak feature. The time needed for such a changeover can subsequently be compared with the timescale of the MZM leakage driven by abrupt coupling of the QD to the topological chain.
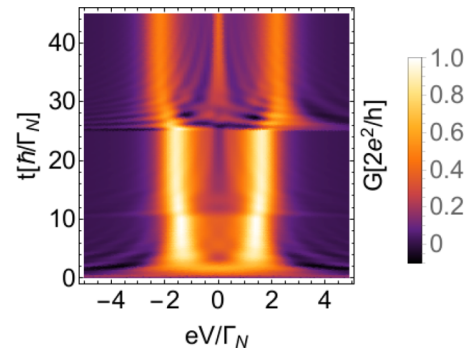

FIG. 5. Time-resolved differential conductance obtained for $\Gamma_S = 3\Gamma_N$, $t_m = 0.5\Gamma_N\theta(t - 10\frac{\hbar}{\Gamma_N})$, and QD energy level $\epsilon_d = 1.5\Gamma_N\theta(t - 25\frac{\hbar}{\Gamma_N})$, where θ is the step function. Like in Fig. 4, we initially couple the QD to the external N/S leads, imposing the energy level $\epsilon_d = 0$. After $t = 10\hbar/\Gamma_N$ the quantum dot is connected to the topological superconductor, inducing the destructive interference ditch in the zero-bias conductance. At $t = 25\hbar/\Gamma_N$ we subsequently lift the QD energy level to $\epsilon_d = \Gamma_N$, and from this moment onward the ditch transforms into the zero-bias peak. This feature establishes after approximately $15\hbar/\Gamma_N$, i.e., at $t \simeq 40\hbar/\Gamma_N$.

For this purpose we consider the following three-step procedure. (i) As before, we start by forming the N-QD-S circuit with the initial energy level $\epsilon_d = 0$ and let the Andreev bound states become established. (ii) Once the differential conductance saturates at its static value (at $t \simeq 10\hbar/\Gamma_N$ fluctuations become almost negligible), we couple the quantum dot to the topological chain. After a certain amount of time the interference ditch appears in the zero-bias conductance. (iii) When 'the dust is settled' we abruptly lift the QD energy level to $\epsilon_d = 1.5\Gamma_N$ by applying the gate voltage. In this way the destructive interference will gradually be replaced by the conventional MZM leakage regime.

We have estimated that this transition takes approximately $\Delta t = 15[\frac{\hbar}{\Gamma_N}]$. Such a timescale to transform one Majorana feature to another is comparable to the time interval needed for the emergence of the zero-energy peak after abrupt coupling of the QD to the topological superconductor (see Fig. 5). Observation of such a dynamical changeover could thus indirectly probe the MZM leakage time itself. In Sec. V we provide a quantitative evaluation of this characteristic time, having in mind the typical energy scales in experiments used with various quantum dots coupled to superconductors and/or topological superconductors.

V. QUANTITATIVE EVALUATIONS

To deliver reliable information on the timescale in tangible units one has to take into account the specific energy scales for the experimentally achievable setups in the analysis of the Andreev/Majorana bound states. Let us consider a few realistic examples.

A. Typical energy scales and timescales

The energy gap of conventional (s-wave) superconductors, which are often used in experiments with quantum dots, varies from a few tens to hundreds of μeV. For instance, the

vanadium electrode used in Ref. [38] was characterized by $\Delta_S \simeq 0.55$ meV. The energy gap of the titanium electrode used by Deacon *et al.* [39] was about 152 μeV. In the present context the proximity-induced on-dot pairing gap, which is roughly equal to Γ_S [35], would be more useful. Its value in the experiment performed by Jünger *et al.* [40] varied from 10 to 165 μeV, whereas in the setup of Deng *et al.* [24] using Ti/Al its magnitude was 250 μeV.

To observe well-pronounced subgap states the hybridization with the metallic electrode Γ_N (which controls the inverse lifetime) should be considerably smaller than both Γ_S and Δ_S. For this reason we have enforced $\Gamma_N \ll \Gamma_S$; otherwise, the in-gap states would overlap with each other. In numerous experiments devoted to investigations of the in-gap bound states, such coupling to the metallic electrode Γ_N was kept about 10 or 100 times smaller than Γ_S. For example, Ref. [38] reported the experimental value $\Gamma_N \simeq 50$ μeV. In our present approach (where Γ_N is used as the energy unit) we thus assume the following realistic value: $\Gamma_N \simeq$ 5–50 μeV, implying the time unit $\frac{\hbar}{\Gamma_N} \simeq 0.125$–1.25 ns. Taking such quantities into account, the time of MZM leakage into the quantum dot region $\simeq 15[\frac{\hbar}{\Gamma_N}]$ (estimated for $t_m = 0.5\Gamma_N$) would be approximately 2–20 ns. Transport measurements have temporal resolution in the subpicosecond regime [13], so this dynamical process should be observable in real time.

One should note that the coupling t_m between the QD and topological superconducting chain is expressed in terms of Γ_N. To reconcile the specific influence of t_m on the Majorana leakage time, we shall briefly analyze in Sec. V B a few representative values. In regard to a quantitative effect of the hybridization Γ_S we have checked that its influence on the Majorana mode leakage time into the QD region is rather negligible.

B. Influence of t_m

Figure 6 shows the time-resolved differential conductance obtained for several values of the dot-chain hybridization t_m. We clearly notice that the zero-energy feature develops more rapidly for stronger couplings t_m. Besides this zero-energy mode one also observes that the Andreev quasiparticle states split into two branches. One of them (the low-energy Andreev branch) is located at $\pm\sqrt{\Delta_d^2 + \epsilon_d^2}$. The other one (high-energy branch), arising from hybridization with the Majorana mode, is formed at $\pm\sqrt{\Delta_d^2 + \epsilon_d^2 + (2t_m)^2}$, in agreement with the static solution predictions [31,32].

To quantify the time interval needed for formation of the zero-energy Majorana feature we have fitted (Fig. 7) the difference between the initial and final ($t = \infty$) zero-bias conductances by an exponential function,

$$G(0,t) = G(0,\infty) - [G(0,\infty) - G(0,t_1)]e^{-(t-t_1)/\tau}, \quad (15)$$

where the initial moment $t_1 = 20$. The phenomenological parameter τ characterizes the temporal interval, in which a mismatch between the initial conductivity and the equilibrium conductance diminishes e times. Values of such a numerically evaluated parameter τ indicate that the development of the MZM features occurs faster the stronger t_m is. A few examples are listed in Table I.
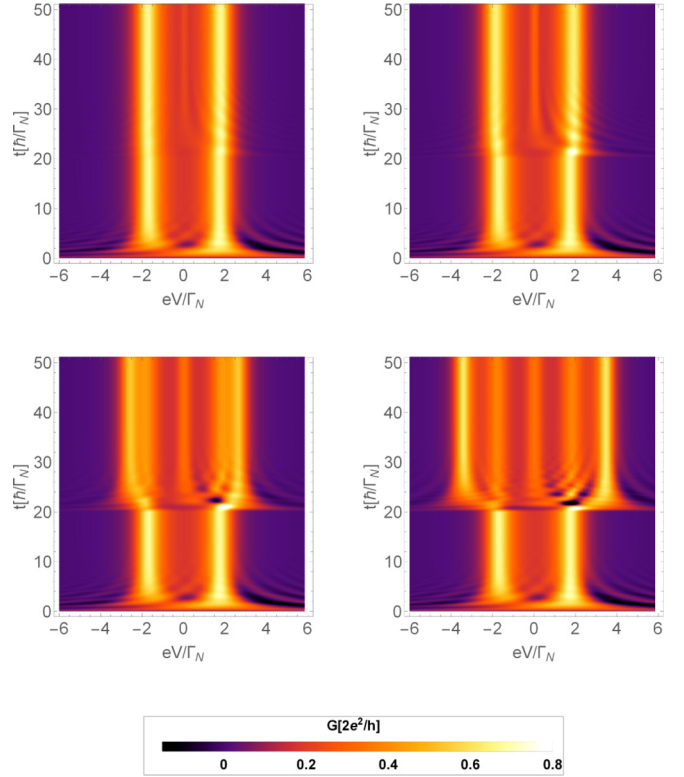

FIG. 6. Evolution of the differential conductance obtained for the setup shown in Fig. 1, assuming the couplings $t_m = 0.25\Gamma_N$ (top left), $0.5\Gamma_N$ (top right), $1\Gamma_N$ (bottom left), $1.5\Gamma_N$ (bottom right). The quantum dot is abruptly hybridized with the Majorana end mode at $t = 20\hbar/\Gamma_N$. We used the model parameters $\Gamma_S = 3\Gamma_N$, $\epsilon_d = \Gamma_N$.

VI. SUMMARY

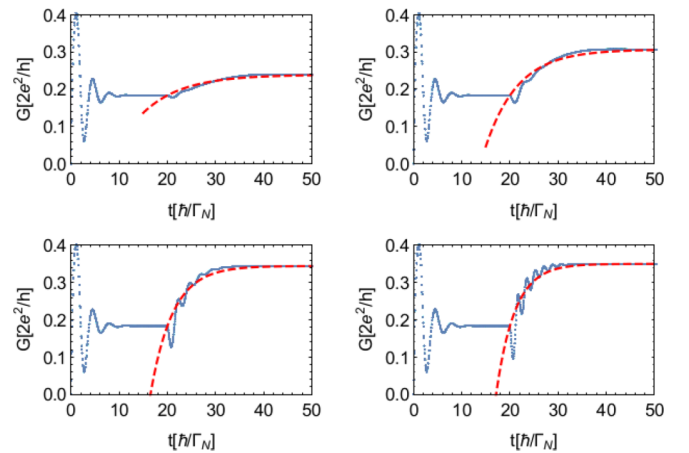We have investigated the time-resolved development of the Majorana features transmitted onto the quantum dot due to

FIG. 7. Blue dots represent the time evolution of the zero-bias differential conductivity obtained for $\Gamma_S = 3\Gamma_N$, energy of the quantum dot $\epsilon_\sigma = \Gamma_N$, and quantum-dot-chain couplings $t_m = 0.25\Gamma_N$ (top left), $0.5\Gamma_N$ (top right), $1\Gamma_N$ (bottom left), $1.5\Gamma_N$ (bottom right). Quantum dot is abruptly connected to Majorana mode at time $t = 20\hbar/\Gamma_N$. Red dashed lines represent exponential fitting function with the characteristic time scale τ.

TABLE I. Leakage time τ obtained for several couplings t_m.

$t_m[\Gamma_N]$	$\tau[\hbar/\Gamma_N]$
0.25	8.2
0.5	6.7
0.75	5.4
1	4.6
1.5	3.8

its coupling to the topological superconductor. For its feasible detection we have considered the tunneling of charge through a circuit in which the quantum dot is strongly hybridized with the bulk superconductor and weakly coupled to the normal metallic lead. Our hybrid structure can be realized in practice, depositing the topological nanowire (for instance, a chain of magnetic *Fe* atoms) with a side-attached quantum dot (e.g., nonmagnetic atom) on the surface of a conventional superconductor [26,41]. Approaching the QD with the conducting STM tip, its low-energy quasiparticles could be observed in the differential conductance, originating from the Andreev (particle-to-hole) scattering that is efficient in the low-bias regime, which is smaller than or comparable to the superconducting gap.

We have evaluated the characteristic time needed for inducing the Majorana features in the zero-bias conductance. When the QD energy level is distant from the chemical potential, the Majorana leakage is manifested by enhancement of the differential conductance. In the opposite limit, when the quantum dot level is near the chemical potential, the Majorana mode has a detrimental influence on the subgap spectrum of the QD, producing the interferometric dip structure. We have evaluated the time interval during which these features emerge after (i) abrupt coupling of the quantum dot to the topological superconducting nanowire and (ii) a sudden change in the quantum dot energy level by the external gate potential. For empirically realistic parameters we have found that the emergence of the Majorana features would take, in both cases, about 2–20 ns, in perfect agreement with estimations obtained by a full counting statistics analysis [11]. This dynamical process should be detectable with the use of currently available state-of-the-art tunneling spectroscopies.

Precise control of the topological superconducting hybrid structures assembled by the STM technique [26] is very promising for measurements of the Majorana and Andreev quasiparticle timescales, e.g., manifested in response to a quench of the energy levels imposed by external gate potentials. The tight-binding parameters (listed in the supplementary information of Ref. [26]) imply the Majorana leakage time is faster than nanoseconds. Obviously, such an effect has not been observed in the stationary STM measurements. Nonetheless, we are confident that time-dependent signatures of the zero-energy (Majorana) and finite-energy (Andreev/Shiba) quasiparticles can be detected for this particular hybrid system, e.g., in response to the gate potential abruptly applied to Co atoms. Under such circumstances the time-dependent differential conductance should reveal the major qualitative features shown by us in Figs. 4 and 5. In summary, the experimental results in Ref. [26] can be

regarded as a proof of concept, confirming that the spatial profile (and, hopefully, dynamical signatures too) of the Majorana modes can be precisely controlled by the state-of-the-art STM method. For feasible means to probe the characteristic timescales, we suggest imposing the steplike gate potentials onto the nontopological part (Co atoms) of this hybrid structure. Such dynamics seems to be fast enough to guarantee the practical realizations of braiding protocols designed for Majorana quasiparticles.

Our estimations have been done for zero temperature, but we have checked that temperature has a negligible influence on the Majorana leakage time. In future studies it would be worthwhile to consider the correlated quantum dot, where the superconducting proximity effect competes with the Coulomb repulsion qualitatively affecting the in-gap bound states. In particular, they may cross one another at the so-called, zero-π transition. Their dynamical interplay with the Majorana mode would require more sophisticated many-body techniques (e.g., a time-dependent numerical renormalization approach), which is beyond a scope of our study.

APPENDIX: EQUATIONS OF MOTION

In this Appendix we present explicitly all the correlation functions appearing in the equation of motion approach when computing the time-dependent QD occupancy $n_\sigma(t)$ and the charge current $I_\sigma(V, t)$. The complete list is given in Table II.

TABLE II. The list of 12 momentum-dependent functions f_{ki} and 9 momentum-independent functions f_i constituting a closed set of the equations of motion.

f_i	f_{ki}
$f_1 = \langle \hat{d}_\uparrow^\dagger(t)\hat{d}_\uparrow(t)\rangle$	$f_{k1} = \langle \hat{d}_\uparrow^\dagger(t)\hat{c}_{k\uparrow}(0)\rangle$
$f_2 = \langle \hat{d}_\downarrow^\dagger(t)\hat{d}_\downarrow(t)\rangle$	$f_{k2} = \langle \hat{d}_\uparrow(t)\hat{c}_{k\downarrow}(0)\rangle$
$f_3 = \langle \hat{f}^\dagger(t)\hat{f}(t)\rangle$	$f_{k3} = \langle d_\uparrow(t)\hat{c}_{k\uparrow}(0)\rangle$
$f_4 = \langle \hat{d}_\downarrow(t)\hat{d}_\uparrow(t)\rangle$	$f_{k4} = \langle d_\downarrow^\dagger(t)\hat{c}_{k\downarrow}(0)\rangle$
$f_5 = \langle \hat{d}_\uparrow^\dagger(t)\hat{f}(t)\rangle$	$f_{k5} = \langle \hat{f}^\dagger(t)\hat{c}_{k\uparrow}(0)\rangle$
$f_6 = \langle \hat{d}_\uparrow^\dagger(t)\hat{f}^\dagger(t)\rangle$	$f_{k6} = \langle \hat{f}(t)\hat{c}_{k\uparrow}(0)\rangle$
$f_7 = \langle \hat{d}_\downarrow(t)\hat{f}(t)\rangle$	$f_{k7} = \langle \hat{f}(t)\hat{c}_{k\downarrow}(0)\rangle$
$f_8 = \langle \hat{d}_\downarrow(t)\hat{f}^\dagger(t)\rangle$	$f_{k8} = \langle \hat{f}^\dagger(t)\hat{c}_{k\downarrow}(0)\rangle$
$f_9 = \langle \hat{d}_\uparrow^\dagger(t)\hat{d}_\downarrow(t)\rangle$	$f_{k9} = \langle \hat{d}_\downarrow(t)\hat{c}_{k\downarrow}(0)\rangle$
	$f_{k10} = \langle \hat{d}_\uparrow^\dagger(t)\hat{c}_{k\downarrow}(0)\rangle$
	$f_{k11} = \langle \hat{d}_\downarrow(t)\hat{c}_{k\uparrow}(0)\rangle$
	$f_{k12} = \langle \hat{d}_\downarrow^\dagger(t)\hat{c}_{k\uparrow}(0)\rangle$

The corresponding set of coupled equations of motion for the momentum-dependent f_{ki} functions is given by

$$\frac{df_{k1}}{dt} = \left(i\epsilon_\uparrow - \frac{\Gamma_N}{2}\right)f_{k1} + i\frac{\Gamma_S}{2}f_{k11} + it_m(f_{k5} + f_{k6}) + iV_k e^{i\xi_k t} f_{FD}[(\xi_k - eV), T],$$

$$\frac{df_{k2}}{dt} = \left(-i\epsilon_\uparrow - \frac{\Gamma_N}{2}\right)f_{k2} - i\frac{\Gamma_S}{2}f_{k4} - it_m(f_{k7} + f_{k8}),$$

$$\frac{df_{k3}}{dt} = \left(-i\epsilon_\uparrow - \frac{\Gamma_N}{2}\right)f_{k3} - i\frac{\Gamma_S}{2}f_{k12} - it_m(f_{k5} + f_{k6}),$$

$$\frac{df_{k4}}{dt} = \left(i\epsilon_\downarrow - \frac{\Gamma_N}{2}\right)f_{k4} - i\frac{\Gamma_S}{2}f_{k2} + iV_k e^{i\xi_k t} f_{FD}[(\xi_k - eV), T],$$

$$\frac{df_{k5}}{dt} = i\epsilon_m f_{k5} + it_m(f_{k1} - f_{k3}),$$

$$\frac{df_{k6}}{dt} = -i\epsilon_m f_{k6} + it_m(f_{k1} - f_{k3}),$$

$$\frac{df_{k7}}{dt} = -i\epsilon_m f_{k7} + it_m(f_{k10} - f_{k2}),$$

$$\frac{df_{k8}}{dt} = i\epsilon_m f_{k8} + it_m(f_{k10} - f_{k2}),$$

$$\frac{df_{k9}}{dt} = \left(-i\epsilon_\downarrow - \frac{\Gamma_N}{2}\right)f_{k9} + i\frac{\Gamma_S}{2}f_{k10},$$

$$\frac{df_{k10}}{dt} = \left(i\epsilon_\uparrow - \frac{\Gamma_N}{2}\right)f_{k10} + i\frac{\Gamma_S}{2}f_{k9} + it_m(f_{k7} + f_{k8}),$$

$$\frac{df_{k11}}{dt} = \left(-i\epsilon_\downarrow - \frac{\Gamma_N}{2}\right)f_{k11} + i\frac{\Gamma_S}{2}f_{k1},$$

$$\frac{df_{k12}}{dt} = \left(i\epsilon_\downarrow - \frac{\Gamma_N}{2}\right)f_{k12} - i\frac{\Gamma_S}{2}f_{k3}, \tag{A1}$$

and for the momentum-independent f_i functions it is correspondingly given by

$$\frac{df_1}{dt} = 2\text{Im}\left[-\frac{\Gamma_S}{2}f_4 + t_m(f_5 + f_6) + S_{k1} - \frac{i\Gamma_N}{2}f_1\right],$$

$$\frac{df_2}{dt} = 2\text{Im}\left[-\frac{\Gamma_S}{2}f_4 + S_{k4} - \frac{i\Gamma_N}{2}f_2\right],$$

$$\frac{df_3}{dt} = 2\text{Im}[t_m(f_6 - f_5)],$$

$$\frac{df_4}{dt} = [-i(\epsilon_\uparrow + \epsilon_\downarrow) - \Gamma_N]f_4 - i\frac{\Gamma_S}{2}(1 - f_1 - f_2) - it_m(f_7 + f_8) + i(S_{k2} - S_{k11}),$$

$$\frac{df_5}{dt} = \left[i(\epsilon_\uparrow - \epsilon_m) - \frac{\Gamma_N}{2}\right]f_5 + i\frac{\Gamma_S}{2}f_7 + it_m(f_3 - f_1) + iS_{k5}^*,$$

$$\frac{df_6}{dt} = \left[i(\epsilon_\uparrow + \epsilon_m) - \frac{\Gamma_N}{2}\right]f_6 + i\frac{\Gamma_S}{2}f_8 + it_m(1 - f_1 - f_3) + iS_{k6}^*,$$

$$\frac{df_7}{dt} = \left[-i(\epsilon_\downarrow + \epsilon_m) - \frac{\Gamma_N}{2}\right]f_7 + i\frac{\Gamma_S}{2}f_5 - it_m(f_4 + f_9) + iS_{k7},$$

$$\frac{df_8}{dt} = \left[-i(\epsilon_\downarrow - \epsilon_m) - \frac{\Gamma_N}{2}\right]f_8 + i\frac{\Gamma_S}{2}f_6 - it_m(f_4 + f_9) + iS_{k8},$$

$$\frac{df_9}{dt} = [-i(\epsilon_\downarrow - \epsilon_\uparrow) - \Gamma_N]f_9 - it_m(f_7 + f_8) + i(S_{k12}^* - S_{k10}), \tag{A2}$$

where $S_{ki} = \sum_k V_k e^{-i\xi_k t} f_{ki}$. We have solved these equations numerically, subject to the initial occupancies $f_1(0) = f_2(0) = 0$ and $f_3(0) = 1$. This choice of initial parameters is not crucial for the asymptotic results obtained in the case $\Gamma_N \neq 0$. Additionally, the values of the functions $f_{4-9}(0)$ and $f_{ki}(0)$ are assumed to be zero, which corresponds to the situation where all parts of our setup are disconnected at $t = 0$.

[1] R. Aguado, Majorana quasiparticles in condensed matter, Riv. Nuovo Cimento **40**, 523 (2017).

[2] R. M. Lutchyn, E. P. A. M. Bakkers, L. P. Kouwenhoven, P. Krogstrup, C. M. Marcus, and Y. Oreg, Majorana zero modes in superconductor-semiconductor heterostructures, Nat. Rev. Mater. **3**, 52 (2018).

[3] E. Prada, P. San-Jose, M. W. A. de Moor, A. Geresdi, E. J. H. Lee, J. Klinovaja, D. Loss, J. Nygård, R. Aguado, and L. P. Kouwenhoven, From Andreev to Majorana bound states in hybrid superconductor-semiconductor nanowires, Nat. Rev. Phys. **2**, 275 (2020).

[4] R. Aguado, A perspective on semiconductor-based superconducting qubits, Appl. Phys. Lett. **117**, 240501 (2020).

[5] X. Liu, X. Li, D.-L. Deng, X.-J. Liu, and S. Das Sarma, Majorana spintronics, Phys. Rev. B **94**, 014511 (2016).

[6] C. Schrade and L. Fu, Majorana Superconducting Qubit, Phys. Rev. Lett. **121**, 267002 (2018).

[7] T. Karzig, C. Knapp, R. M. Lutchyn, P. Bonderson, M. B. Hastings, C. Nayak, J. Alicea, K. Flensberg, S. Plugge, Y. Oreg, C. M. Marcus, and M. H. Freedman, Scalable designs for quasiparticle-poisoning-protected topological quantum computation with Majorana zero modes, Phys. Rev. B **95**, 235305 (2017).

[8] S. Hoffman, C. Schrade, J. Klinovaja, and D. Loss, Universal quantum computation with hybrid spin-Majorana qubits, Phys. Rev. B **94**, 045316 (2016).

[9] K. Flensberg, Non-Abelian Operations on Majorana Fermions via Single-Charge Control, Phys. Rev. Lett. **106**, 090503 (2011).

[10] J. F. Steiner and F. von Oppen, Readout of Majorana qubits, Phys. Rev. Res. **2**, 033255 (2020).

[11] R. Seoane Souto, K. Flensberg, and M. Leijnse, Timescales for charge transfer based operations on Majorana systems, Phys. Rev. B **101**, 081407(R) (2020).

[12] T. Posske, C.-K. Chiu, and M. Thorwart, Vortex Majorana braiding in a finite time, Phys. Rev. Res. **2**, 023205 (2020).

[13] R. Tuovinen, E. Perfetto, R. van Leeuwen, G. Stefanucci, and M. A. Sentef, Distinguishing Majorana zero modes from impurity states through time-resolved transport, New J. Phys. **21**, 103038 (2019).

[14] L. Mazza, M. Aidelsburger, H.-H. Tu, N. Goldman, and M. Burrello, Methods for detecting charge fractionalization and winding numbers in an interacting fermionic ladder, New J. Phys. **17**, 105001 (2015).

[15] C. Wang, P. Zhang, X. Chen, J. Yu, and H. Zhai, Scheme to Measure the Topological Number of a Chern Insulator from Quench Dynamics, Phys. Rev. Lett. **118**, 185701 (2017).

[16] C. Yang, L. Li, and S. Chen, Dynamical topological invariant after a quantum quench, Phys. Rev. B **97**, 060304(R) (2018).

[17] M. Maffei, A. Dauphin, F. Cardano, M. Lewenstein, and P. Massignan, Topological characterization of chiral models through their long time dynamics, New J. Phys. **20**, 013023 (2018).

[18] X.-Q. Li and L. Xu, Nonlocality of Majorana zero modes and teleportation: Self-consistent treatment based on the Bogoliubov–de Gennes equation, Phys. Rev. B **101**, 205401 (2020).

[19] T. Jonckheere, J. Rech, A. Zazunov, R. Egger, A. L. Yeyati, and T. Martin, Giant Shot Noise from Majorana Zero Modes in Topological Trijunctions, Phys. Rev. Lett. **122**, 097003 (2019).

[20] J. Manousakis, C. Wille, A. Altland, R. Egger, K. Flensberg, and F. Hassler, Weak Measurement Protocols for Majorana Bound State Identification, Phys. Rev. Lett. **124**, 096801 (2020).

[21] R. Radgohar and M. Kargarian, Effects of dynamical noises on Majorana bound states, Phys. Rev. B **102**, 165111 (2020).

[22] V. Perrin, M. Civelli, and P. Simon, Discriminating Majorana from Shiba bound-states by tunneling shot-noise tomography, arXiv:2011.06893.

[23] T. Mizoguchi, Y. Kuno, and Y. Hatsugai, Detecting Bulk Topology of Quadrupolar Phase from Quench Dynamics, Phys. Rev. Lett. **126**, 016802 (2021).

[24] M. T. Deng, S. Vaitiekenas, E. B. Hansen, J. Danon, M. Leijnse, K. Flensberg, J. Nygård, P. Krogstrup, and C. M. Marcus, Majorana bound state in a coupled quantum-dot hybrid-nanowire system, Science **354**, 1557 (2016).

[25] M.-T. Deng, S. Vaitiekėnas, E. Prada, P. San-Jose, J. Nygård, P. Krogstrup, R. Aguado, and C. M. Marcus, Nonlocality of Majorana modes in hybrid nanowires, Phys. Rev. B **98**, 085125 (2018).

[26] L. Schneider, S. Brinker, M. Steinbrecher, J. Hermenau, T. Posske, M. dos Santos Dias, S. Lounis, R. Wiesendanger, and J. Wiebe, Controlling in-gap end states by linking nonmagnetic atoms and artificially-constructed spin chains on superconductors, Nat. Commun. **11**, 4707 (2020).

[27] H. Pan and S. Das Sarma, Physical mechanisms for zero-bias conductance peaks in Majorana nanowires, Phys. Rev. Res. **2**, 013377 (2020).

[28] D. Crawford, E. Mascot, D. K. Morr, and S. Rachel, High-temperature Majorana fermions in magnet-superconductor hybrid systems, Phys. Rev. B **101**, 174510 (2020).

[29] E. Vernek, P. H. Penteado, A. C. Seridonio, and J. C. Egues, Subtle leakage of a Majorana mode into a quantum dot, Phys. Rev. B **89**, 165314 (2014).

[30] H. Pan, W.S. Cole, J. D. Sau, and S. Das Sarma, Generic quantized zero-bias conductance peaks in superconductor-semiconductor hybrid structures, Phys. Rev. B **101**, 024506 (2020).

[31] J. Barański, A. Kobiałka, and T. Domański, Spin-sensitive interference due to Majorana state on the interface between normal and superconducting leads, J. Phys.: Condens. Matter **29**, 075603 (2016).

[32] T. Zienkiewicz, J. Barański, G. Górski, and T. Domański, Leakage of Majorana mode into correlated quantum dot nearby its singlet-doublet crossover, J. Phys.: Condens. Matter **32**, 025302 (2019).

[33] A. M. Calle, M. Pacheco, P. A. Orellana, and J. A. Otalora, Fano-Andreev and Fano-Majorana correspondence in quantum dot hybrid structures, Ann. Phys. (Berlin, Ger.) **532**, 1900409 (2020).

[34] J. Bauer, A. Oguri, and A.C. Hewson, Spectral properties of locally correlated electrons in a Bardeen–Cooper–Schrieffer superconductor, J. Phys.: Condens. Matter **19**, 486211 (2007).

[35] J. Barański and T. Domański, In-gap states of a quantum dot coupled between a normal and a superconducting lead, J. Phys.: Condens. Matter **25**, 435305 (2013).

[36] Y. Yamada, Y. Tanaka, and N. Kawakami, Interplay of Kondo and superconducting correlations in the nonequilibrium Andreev transport through a quantum dot, Phys. Rev. B **84**, 075484 (2011).

[37] R. Taranko and T. Domański, Buildup and transient oscillations of Andreev quasiparticles, Phys. Rev. B **98**, 075420 (2018).

[38] E. J. H. Lee, X. Jiang, M. Houzet, R. Aguado, C. M. Lieber, and S. De Franceschi, Spin-resolved Andreev levels and parity crossings in hybrid superconductor–semiconductor nanostructures, Nat. Nanotechnol. **9**, 79 (2013).

[39] R. S. Deacon, Y. Tanaka, A. Oiwa, R. Sakano, K. Yoshida, K. Shibata, K. Hirakawa, and S. Tarucha, Tunneling Spectroscopy of Andreev Energy Levels in a Quantum Dot Coupled to a Superconductor, Phys. Rev. Lett. **104**, 076805 (2010).

[40] C. Jünger, A. Baumgartner, R. Delagrange, D. Chevallier, S. Lehmann, M. Nilsson, K. A. Dick, C. Thelander, and C. Schönenberger, Spectroscopy of the superconducting proximity effect in nanowires using integrated quantum dots, Commun. Phys. **2**, 76 (2019).

[41] H. Kim, A. Palacio-Morales, T. Posske, L. Rózsa, K. Palotás, L. Szunyogh, M. Thorwart, and R Wiesendanger, Toward tailoring Majorana bound states in artificially constructed magnetic atom chains on elemental superconductors, Sci. Adv. **4**, eaar5251 (2018).